

Bridge-Enhanced Nanoscale Impedance Microscopy on Organic Light-Emitting Diodes

Undergraduate Researcher
Zhiyang Wei, Northwestern University

Faculty Mentor
Mark C. Hersam
Department of Materials Science and Engineering, Northwestern University

Graduate Student Mentor
Liam S. C. Pingree
Department of Materials Science and Engineering, Northwestern University

Abstract

The use of a variable resistor-capacitor (RC) bridge circuit was previously reported to be a viable solution to the spurious contribution of fringe capacitance during nanoscale impedance microscopy (NIM). In this paper, a refinement of this technique combined with standard NIM is presented as an impedance characterization tool for organic light-emitting diodes (OLEDs). In this technique, a sinusoidal bias is split into two equal branches, which are subsequently sent to the tunable RC circuit and the sample. By balancing the phase and magnitude of the two branches, the contribution to the current through the sample/tip junction can be directly monitored. To demonstrate the improved detection limit offered by this technique over more conventional NIM, conductive AFM measurements were performed on $8\ \mu\text{m}$ by $8\ \mu\text{m}$ OLED devices, demonstrating significant improvement in resolution in the current and phase maps. This paper also suggests possible future research that is necessary to fully enable impedance spectroscopy at the nanoscale.

Introduction

Recent progress in the development of organic light-emitting diodes has led to the realization of OLEDs with power efficiency and color tenability that are adequate for commercialization; however, device stability is still a major problem.¹ As the size of OLEDs continues to shrink, significant device-to-device nonuniformities may occur due to fabrication- and materials-dependent micro- and nanoscopic spatial variations. These nonuniformities may lead to reduced overall system performance, such as “dark spots” at various locations in the device that exhibit little or no electroluminescence. Conductive atomic force microscopy (cAFM) has been effective at probing current flow and resistivity variations with nanometer scale spatial resolution in a variety of materials and devices.^{2–6} In this method, a conductive AFM tip is brought into contact with the gold/aluminum cathode

of the sample, which is subject to an external bias applied to the glass/ITO layer. Profiles of distinctive individual OLED devices have been obtained with current, topography, and electroluminescence mapping under direct current (DC) bias.⁷ In these maps, device-to-device variations in light emission and current flow have been seen.

Another cAFM technique — nanoscale impedance microscopy (NIM) — was recently developed as a characterization tool of nanoelectronic devices and circuits.⁸ NIM concurrently monitors the amplitude and phase response of the current through a cAFM tip in response to a temporally periodic applied bias. By varying the frequency of the driving potentials, the resistance and reactance of conductive pathways can be quantitatively determined.⁸ In this technique, an alternating current (AC) is applied to the sample, and the resulting amplitude

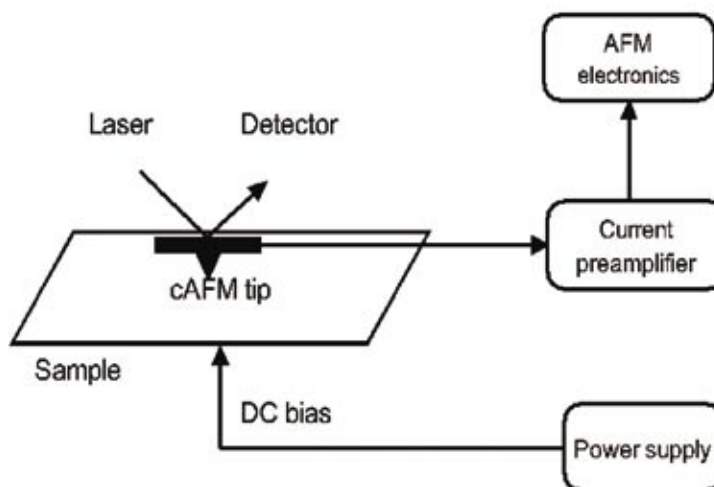


Figure 1: Schematic diagram of cAFM measurement under dc bias.

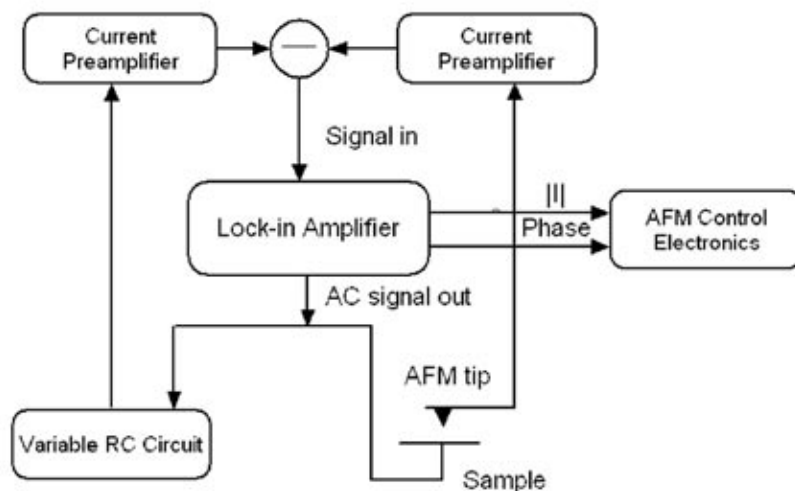


Figure 2: A block diagram of BE-NIM apparatus. An ac bias originating from the LIA is subsequently split into two branches, one of which is sent to the variable RC circuit while the other is fed to the sample. The current and phase of the difference between the two branches are measured by the LIA and exported to the AFM control electronics.

and phase response of the current at the driving frequency is monitored by a cAFM tip and analyzed with a lock-in amplifier. However, the resolution of this technique is limited by the fringe capacitance between the sample and the probing compartment. Theoretically the fringe capacitance can be modeled as a parallel capacitor that consists of two plates, one of which is the ITO sheet of the sample, and the other is the non-apex region of the cantilever. The additional current flow due to the fringe capacitance convolves with the current flow through the tip/sample junction, resulting in corrupted current and phase shift maps.

A previous experiment⁹ presented the use of a variable resistor-capacitor (RC) circuit to compensate for the spurious contribution to the AC flow by fringe capacitance in NIM measurements. By analogy to the variable RC components in electrical bridge circuits, this technique was referred to as bridge enhanced nanoscale impedance

microscopy (BE-NIM). In this experiment, cAFM scanning was performed on gold electrodes patterned on silicon oxide grown on n-type silicon at a single AC bias and frequency. It was demonstrated that with BE-NIM, the detection limit of NIM could be improved by at least several orders of magnitude. Here we present a refined BE-NIM technique that is applicable to operational OLEDs for the first time. This work may lead to future development in impedance study at various frequencies.

Background

Electroluminescence (EL) — the generation of light (other than black-body radiation) from condensed matter by electrical excitation — has been investigated in organic molecular solids since the 1950s.¹⁰ OLEDs follow the same light-emitting principle as traditional LEDs. When an electron from the electron-transport material combines with a hole from the hole-transport material, a

photon is emitted. The main difference between OLEDs and traditional LEDs is that the electron- and hole-transport materials are organic solids instead of inorganic ones. Practical commercialization of these early devices was limited due to several obstacles, including the high operating voltage as a consequence of the crystal thickness in the micrometer range, in addition to the difficulties in producing stable and consistent devices. A significant improvement on organic electroluminescent devices was made in the 1970s by the use of thin organic films prepared by vacuum vapor deposition or the Langmuir-Blodgett technique instead of single crystals.^{11–13} As a result of the reduced organic layer thickness, the same electric field was achieved with a much lower operating voltage. True potential for applications of OLEDs in lighting and display devices were demonstrated by Tang et al. using multilayer structures that considerably enhanced the efficiency of light emission by achieving a better balance of the number of charge carriers

of opposite sign and further lowered the operating voltage by reducing the mismatch of energy levels between the organic materials and the electrodes.^{14,15} Improvements in materials and device architecture have resulted in devices with luminance exceeding 100000 cd/m² and external quantum efficiencies in excess of 4%.¹⁶ Since the end of 1990s, OLEDs have entered the stage of commercialization and are considered promising candidates for the next generation of large-area flat-panel displays.^{17,18}

Although it has been reported that high luminance and efficiencies¹⁹ can be achieved with OLEDs that may enable future technological applications, the insufficient lifetime and the necessity for encapsulation of these devices still pose significant difficulties for their true commercialization. Moreover, both electroluminescent intensity and efficiency decrease during operation, in addition to the formation and growth of nonemitting areas (“dark spots”) accompanied by increasing resistances of the devices.^{20,21} To arrive at a better description of the electrical properties of organic light-emitting systems, equivalent circuits are often used. Using impedance microscopy, it was found that two parallel RC components connected in series are required for the description of two-layer devices,²² where an NPB layer is used as the hole transporter and an Alq layer as the electron carrier.

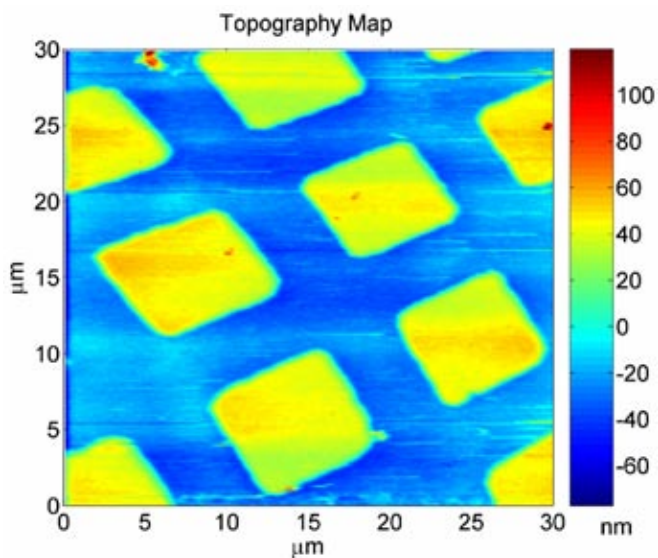


Figure 3(a): Topography map of the OLED array collected at an applied dc bias of 18V and a set point force of 15nN.

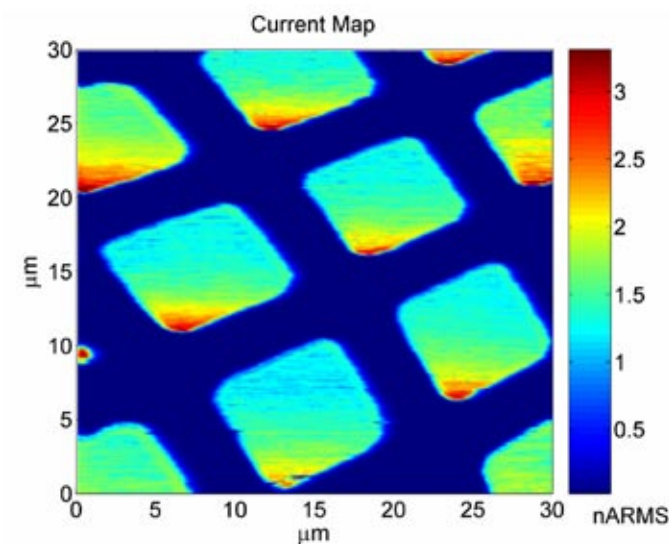


Figure 3(b): Current map of the OLED array collected at an applied dc bias of 18V and a set point force of 15nN.

Approach

Sample Preparation

The fabrication of OLEDs used in the experiment is achieved in the following procedure. Indium-tin-oxide (ITO) glass slides with a sheet resistance of $< 30 \Omega/\text{cm}$ from Thin Film Devices were cleaned and used as a substrate.²³ The hole-transport material α -NPB [*N,N'*-di(α -naphthyl)-*N,N'*-diphenyl-1,1'-biphenyl-4,4'-diamine)] and the electron-transport/emissive material Alq [tris(8-hydroxyquinolato) aluminum(III)]²⁴ were purified by gradient sublimation prior to use. The NPB and Alq layers were then thermally deposited at a rate of $1.5 - 2.0 \text{ \AA/s}$ to a thickness of 25 and 30 nm, respectively, at a base pressure of 10^{-7} Torr. The cathode consists of a silver layer also deposited by thermal evaporation. A stencil mask consisting of a 2000-mesh copper transmission electron microscopy grid (Ted Pella,

Inc.) was used to define the $8 \mu\text{m}$ by $8 \mu\text{m}$ dimension of the cathode. In a similar cAFM experiment previously done by the Hersam group, a 12 nm gold layer was deposited on top of a 60 nm aluminum layer to prevent oxidation of aluminum during the experiment. However, due to slight variations in cathode source location during evaporation of the aluminum and gold, these metal layers were slightly misaligned or offset. In this experiment, a single silver layer is used as the cathode in the hope of avoiding the misalignment.

DC Characterization of Samples

Prior to making impedance measurements under an AC bias, DC characterization was performed to ensure that the newly fabricated devices with silver cathodes respond to the DC bias in the same way as devices deposited with gold/aluminum cathodes. A schematic of the apparatus is shown in

Figure 1, as previously reported in an article by Pingree et al.⁷ Scanning was performed with a Thermomicroscope CP Research AFM in ambient conditions. Titanium-doped, platinum-coated AFM Ultrasharp™ tips from MikroMasch were used in the measurements. Current flow through the tip-sample junction was detected with a DL Instruments 1212 current preamplifier and converted to a digital signal with an analog-to-digital converter. The same sample and AFM tips would be used in the next stage of the experiment, AC characterization with BE-NIM.

Bridge Characterization

Fringe capacitance, which acts in parallel with the tip/sample junction, has been reported to range from 1 to 100 pF.^{25,26} In our apparatus, we chose three air-variable capacitors whose range of capacitance matched that of the fringe

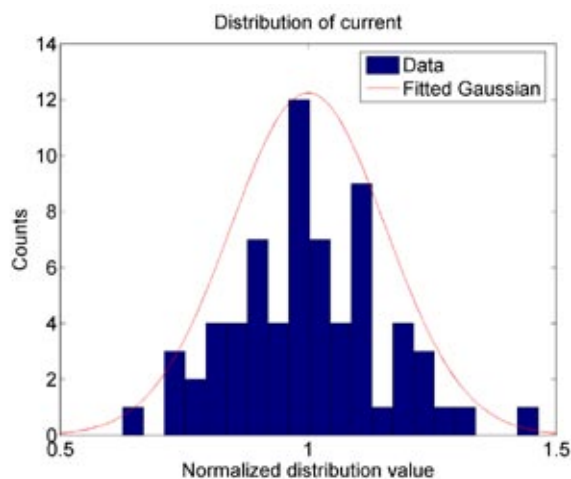


Figure 4(a): Normalized distribution of current for 68 OLEDs with Ag cathodes. Current values are normalized to the mean.

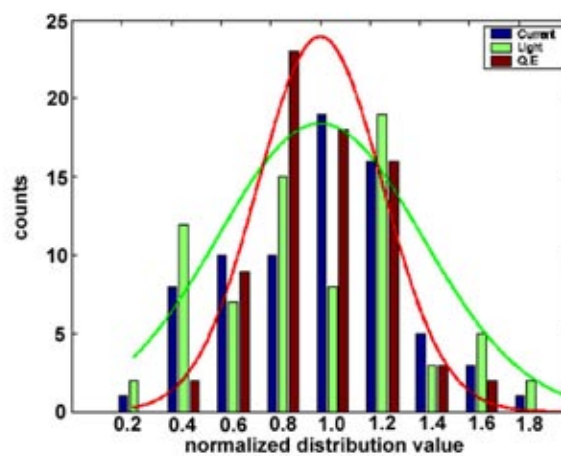


Figure 4(b): Normalized distribution of light emission, current, and quantum efficiency for 74 OLEDs with Au/Al cathodes.²⁷

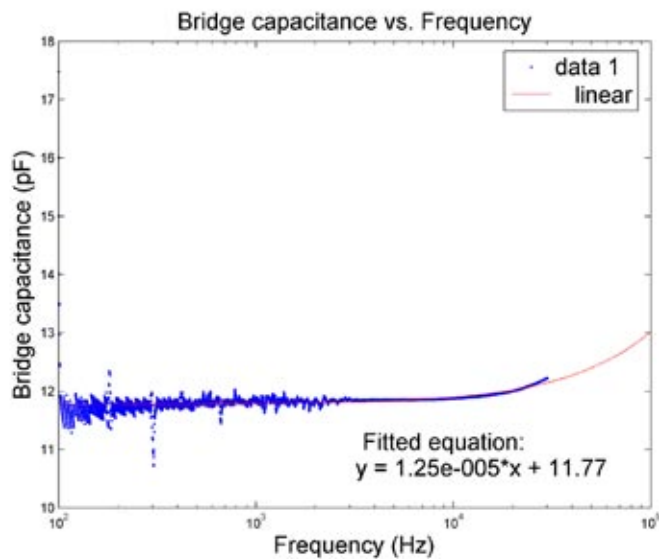


Figure 5(a): Plot of bridge capacitance as a function of frequency for frequencies from 100 Hz to 30 kHz.

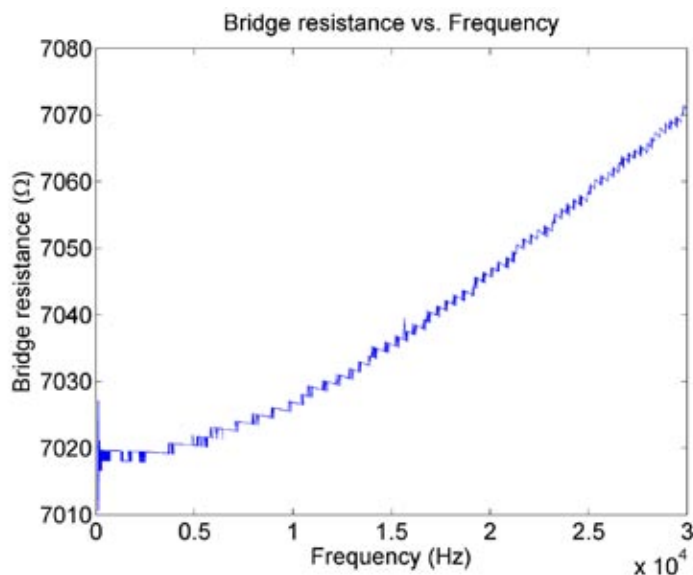


Figure 5(b): Plot of bridge resistance as a function of frequency for frequencies from 100 Hz to 30 kHz.

capacitance when connected in series. Each of the capacitors consisted of four metal plates, two of which could be finely tuned with a knob connected to the shaft. These two plates complemented the other two and increased capacitance when turned in one section and vice versa. The capacitors were then connected to three resistors in series, with resistances of 1 kΩ, 1 kΩ, and 5 kΩ, respectively. Despite the fact that capacitance and resistance are generally considered to be frequency independent, it was necessary to perform some tests to ensure that this was indeed the case in our setup. This was especially true for the capacitors, since interaction between plates spaced further apart might be negligible at low frequencies, but become significant at higher frequencies, thus exhibiting frequency-dependent behavior. The characterization of the bridge was accomplished by performing frequency sweeps on the capacitor and resistor circuits for a long range of frequencies, which was 500 Hz to 30 kHz in our case. If any nonidealities existed in the circuits, variations in measured capacitance or impedance would be observed on a capacitance-frequency or an impedance-frequency plot. After the bridge was verified to behave ideally, it was added to the circuit to complete the construction of the experimental setup.

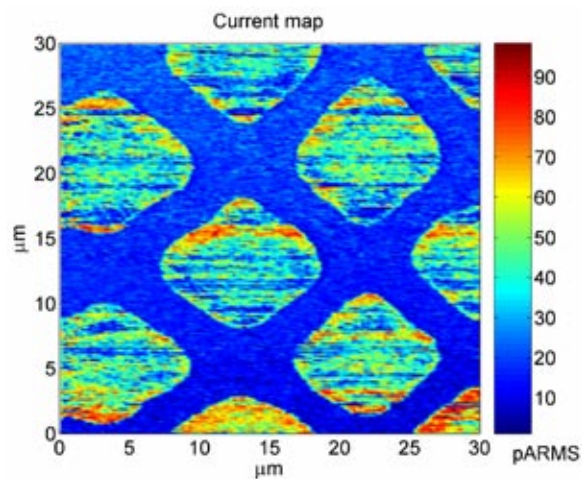


Figure 6(a): Current map collected at 0.15V ac bias, 4 kHz frequency, 0V dc bias, and 15nN set point force with BE-NIM.

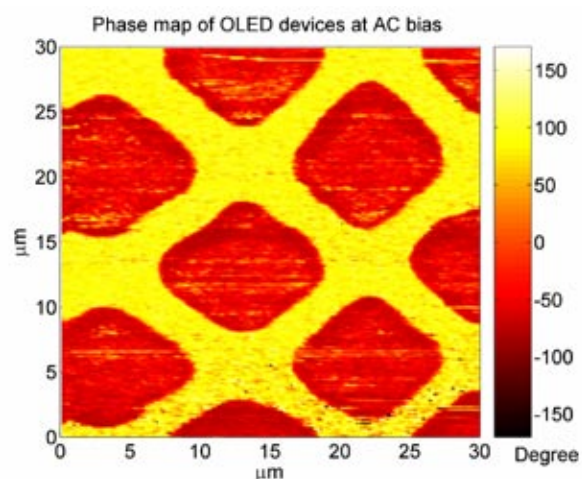


Figure 6(b): Phase map collected at 0.15V ac bias, 4 kHz frequency, 0V dc bias, and 15nN set point force with BE-NIM

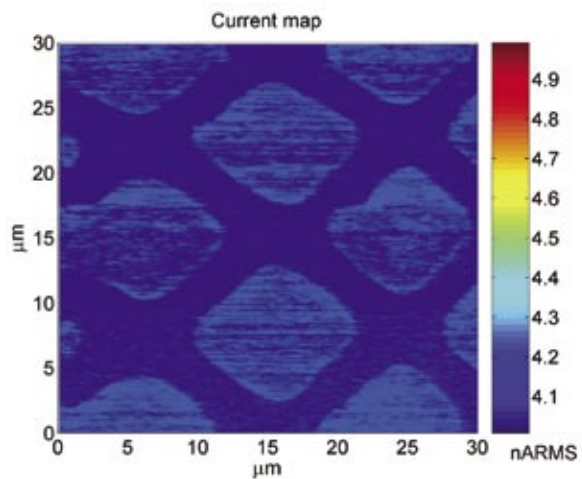


Figure 6(c): Current map collected at 0.15V ac bias, 4 kHz frequency, 0V dc bias, and 15nN set point force with the conventional nonbridge NIM.

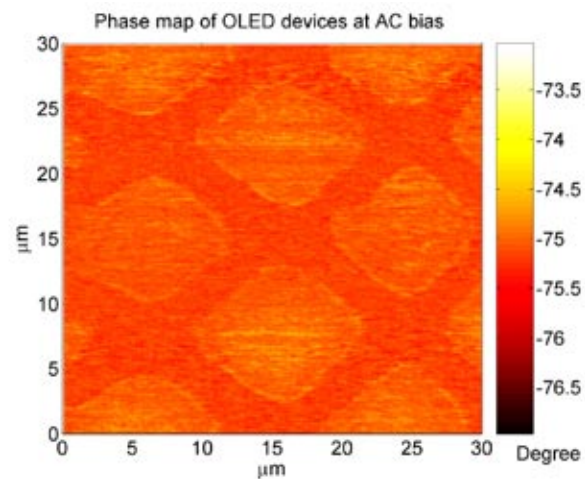


Figure 6(d): Phase map collected at 0.15V ac bias, 4 kHz frequency, 0V dc bias, and 15nN set point force with the conventional nonbridge NIM.

Bridge Enhanced Nanoscale Impedance Microscopy

The apparatus of BE-NIM was originally proposed in the work by L. S. C. Pingree et al. in 2005. A schematic of this technique is shown in Figure 2. In this experiment, an oscillatory driving signal was generated by a Stanford Research Systems SR 850 DSP lock-in amplifier (LIA) and was subsequently split into two equal signals at a T-junction. One branch of the signal was directed to the AFM as the driving AC bias, whereas the other branch was sent to the variable RC bridge. Conductive AFM measurements were made with titanium-doped, platinum-coated tips in ambient conditions. Using two independent DL Instruments 1212 current preamplifiers, the current from both branches was monitored. Subsequently the sample and bridge signals were sent back to the A and B inputs of the LIA, respectively. To obtain impedance maps of the sample, the magnitude and phase outputs of the LIA were routed to the AFM control electronics. To circumvent the problem of fringe capacitance, a preliminary scan was performed to obtain a topography map of the sample. After the topography map was collected, the AFM tip was then moved to a non-OLED region where it was directly in contact with the organics, offering only a high resistance pathway for current to flow through the sample/tip junction. The variable RC bridge was tuned at this time to minimize the magnitude and phase of the signal detected by the LIA, which would be the current flow caused by fringe capacitance. Contact mode cAFM was commenced subsequently. If the bridge was tuned precisely so that it could balance out the fringe capacitance, the

difference of A-B would be, in principle, the current flow purely contributed to by the tip-sample junction.

To prepare the experimental apparatus for impedance spectroscopy, frequency sweeps were performed on the current preamplifiers as well as fringe impedance to determine their response with respect to frequency. This was necessary because any frequency-dependent behavior in the experimental apparatus and fringe impedance would disturb the bridge balance, and any unbalanced portion of the signal would convolve with the current flow in the device, contributing additional magnitude and phase shift to the measurements. The current preamplifier had a gain setting of 10^6 in all of the following frequency sweeps.

Results

DC Characterization of Samples

Under a driving DC voltage of 18V, topography and current maps were collected as shown in Figure 3(a) and 3(b). Histograms of current were compared with those obtained using boron-doped, diamond-coated tips on OLED devices with gold/aluminum cathodes. As evident in Figure 4(a) and 4(b),²⁷ no additional variations are introduced though the use of Ag cathodes, although slight reduction in device performance was expected due to the differences in cathodes and AFM tips. A fitted Gaussian distribution is also included in the figures. The values are normalized to the mean, and the standard deviation is 0.1564. The true mean and standard deviation are 1.3616nA and 0.2129nA, respectively. This stage of the experiment demonstrated that the switch from gold/aluminum cathodes to silver ones was successful and the misalignment

problem was solved. In addition, the Ti/Pt tips proved to be a good substitute to boron-doped, diamond-coated tips.

Bridge Characterization

AC sweeps were done for a range of frequencies between 100 Hz and 30 kHz, and the current and phase data were collected for several capacitance and resistance configurations. One set of data is included in Figure 5. The slope of the C-f was less than 10^{-5} pF, whereas the variation in resistance over the frequency range was only 60Ω , assuring that the variations in capacitance and resistance were small enough to be negligible in our measurements.

BE-NIM

To evaluate the effectiveness of this technique, several batches of $8\ \mu\text{m}$ by $8\ \mu\text{m}$ OLED devices were imaged under a driving AC signal of $0.15\ V_{\text{RMS}}$ having a frequency of 4 kHz, at a scanning rate of 0.75 Hz with a contact force of 20 nN and a DC bias of 0 V. At zero DC bias, the OLED devices are expected to behave like a simple capacitor, where the two plates of the capacitor would be the ITO anode and the silver cathode, and the NPB and Alq layers would act as the dielectric materials. Therefore, the current would be one quarter of a period behind of the voltage, or -90° out of phase with the driving signal.²⁸ The recorded current magnitude and phase maps are shown in Figure 6(a) and 6(b). It can be clearly seen that the improved technique was able to capture the elevated current flow on the OLED devices as well as the phase shift as expected of a capacitor. In addition, validity of these measurements can be confirmed quantitatively by comparing the current magnitude obtained experimentally with the theoretical value. According to elementary circuit

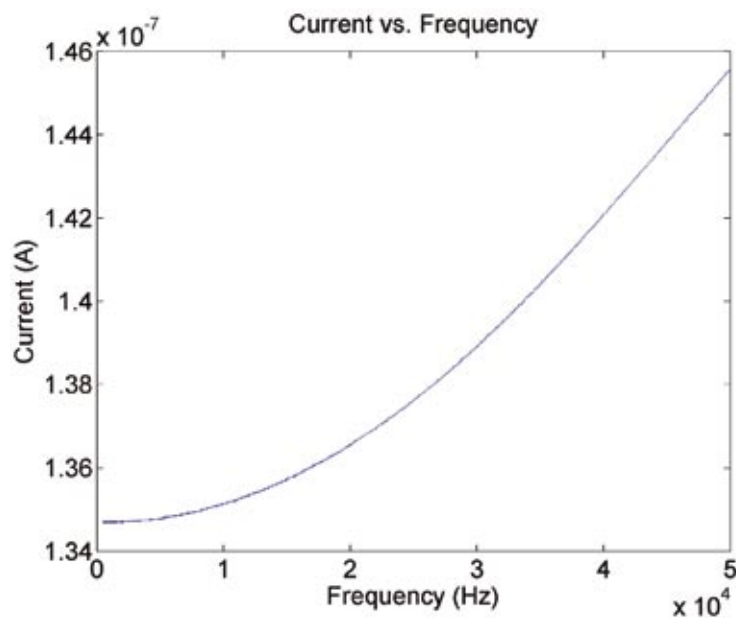


Figure 7(a): Current flow through a 1 MΩ resistor as a function of frequency detected with a DL 1212 current preamplifier at a gain setting of 10⁶ and applied ac bias of 0.15V for frequencies from 500 Hz to 50 kHz.

theory, the magnitude of current flow through a simple capacitor, $|I|$, is given by $|I| = 2\pi fCV$, where C is the capacitance, f is the frequency, and V is the magnitude of the AC bias. The theoretical value of capacitance can be calculated using $C = \epsilon\epsilon_0 A/d$, where $\epsilon \approx 3.5$ is the dielectric constant of the NPB and Alq layers, ϵ_0 is the permittivity of free space, A is the area of each individual OLED device, and d is the combined thickness of the NPB and Alq layers. Using these equations, the theoretical capacitance is approximately 36 fF and the current is approximately $1.3595 \times 10^{-10} A_{RMS}$, whereas the mean of the measured current was $5.58 \times 10^{-11} A_{RMS}$, giving a measured capacitance value of 14.8 fF. The experimental data and theoretical value matched within an order of magnitude. The deviation of the

measured current magnitude from the theoretical value could be attributed to several causes, such as nonuniformities in device performance as suggested by the bell-shaped DC characteristics, device degradation in ambient conditions, and tip resistance. Moreover, a small overhead of the signal above zero when tuning the bridge to null the fringe capacitance could also reduce the strength of the current recorded. Good agreement is also seen for the phase shift detected on the OLED devices, which has a mean of -78.8° . In addition to the possible causes of error listed above, the internal phase shift of the current preamplifiers may have also skewed the experimental data.

To provide a visual comparison of spatial resolution, maps obtained using the standard non-BE-NIM technique are also included in Figure 6(c) and 6(d).

It can be seen that the images obtained with the standard NIM technique show minimal contrast in current and phase between the device and the ITO background. The fringe capacitance, which acted in parallel with the device capacitance, clearly added to the magnitude and phase shift of the current flow and was the dominant contribution, as evident by the approximately $4nA_{RMS}$ magnitude and -75° phase shift. The value of fringe capacitance is calculated to be approximately 1.1pF with the following equation:

$$C = \frac{I}{2\pi fV \sin \theta}$$

where I is the magnitude of current, V is the driving voltage, f is the frequency, and θ is the phase shift.

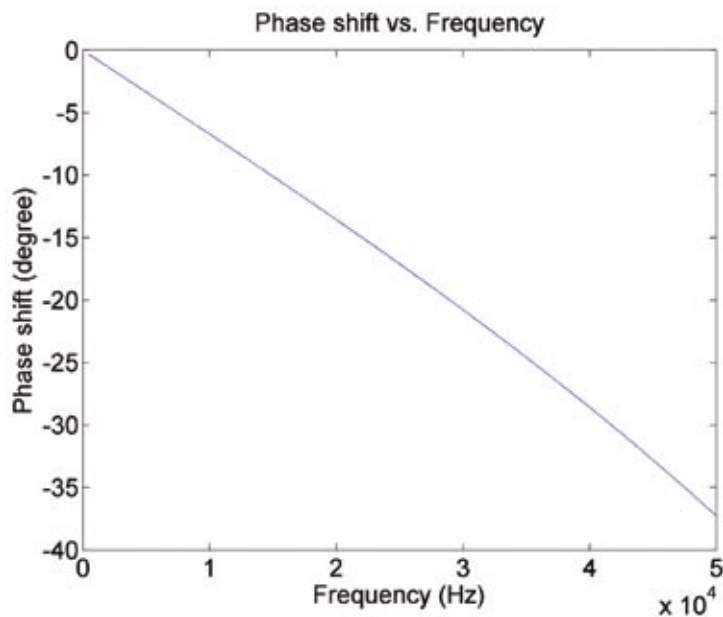


Figure 7(b): Phase shift of the current flow through a $1\text{ M}\Omega$ resistor detected with a DL 1212 current preamplifier at a gain setting of 10^6 and an applied ac bias of 0.15V for frequencies from 500 Hz to 50 kHz .

The improvement of BE-NIM over the standard NIM technique can also be evaluated quantitatively. It was previously stated²⁹ that in NIM, if the ratio of $I_{\text{sample}}/I_{\text{fringe}} > 200$, the phase contribution of the sample will be correctly reflected in the measurement. However, if $I_{\text{sample}}/I_{\text{fringe}} < 100$, the contribution of the fringe capacitance becomes dominant and corrupts the phase signal. In our case, $I_{\text{sample}}/I_{\text{fringe}}$ is approximately 0.01 , indicating at least a 4 order of magnitude improvement in the detection limit of NIM.

Figure 7(a) and 7(b) demonstrate the nonideal behavior of the current preamplifiers. Both the magnitude and phase shift of the current flow detected with the current preamplifiers show significant variations, which are not expected from a pure resistor. In addition, Figure

8 shows a Cole-Cole plot of the fringe impedance for frequencies from 5 kHz to 50 kHz . This plot suggests that the fringe capacitance is not constant throughout the frequencies and that there may be other elements in the system with frequency-dependent capacitance and resistance. With the current equipment limitations and the nonideal behavior of both the fringe capacitance and current preamplifiers, variable frequency sweeps are not possible at this time. Therefore more investigation of these two elements is necessary. Mathematical modeling may be used to unveil the hidden frequency-dependent elements, which could lead to the construction of a more sophisticated bridge circuit than a simple series RC one and enable variable frequency measurements without user intervention.

Conclusions

This work demonstrates the use of a series RC circuit in the cancellation of fringe capacitance during NIM measurements. Although the application of a bridge circuit has been reported elsewhere to serve similar purposes,²⁹ this was the first time the technique was used on operational OLEDs. At a fixed bias and frequency, this technique was capable of greatly improving the spatial resolution of current and phase mapping.

Moreover, the BE-NIM technique can be considered a promising candidate for impedance spectroscopy at the nanoscale. Ideally, frequency sweeps on the OLED devices would provide useful information on the variation of the internal electric field in the devices with frequency. However, it is found that there are other

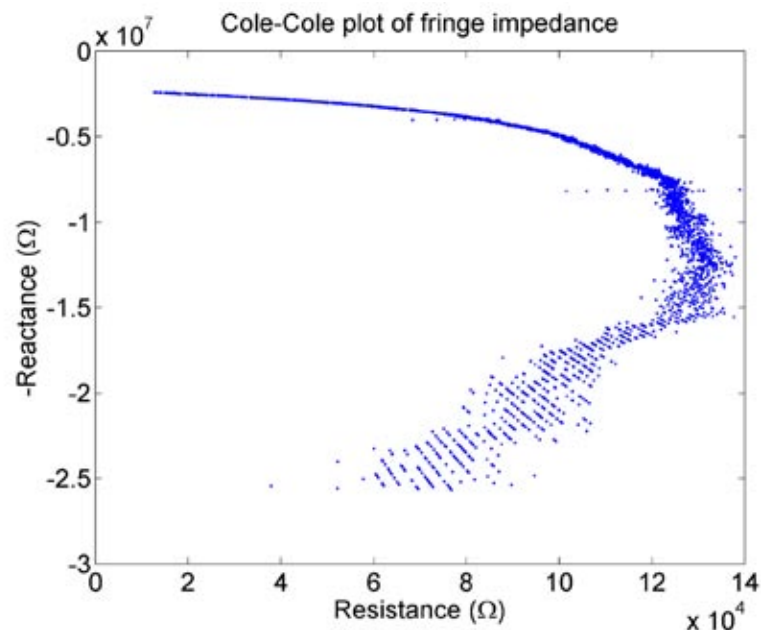


Figure 8: Cole-Cole plot of fringe impedance for frequencies from 5 kHz to 50 kHz.

frequency-dependent factors in the apparatus that prevent us from obtaining accurate results from impedance studies at a range of frequencies. In conclusion, although the BE-NIM technique is currently limited to measurements at a single bias and frequency, it has true potential for future impedance characterization of organic light-emitting diodes at various frequencies.

References

- (1) Aziz, H.; Popovic, Z.; Tripp, C. P.; Hu, N.; Hor, A.; Xu, G. *Appl. Phys. Lett.* **1998**, *72*, 2642.
- (2) Hersam, M. C.; Hoole, A. C. F.; O'Shea, S. J.; Welland, M. E. *Appl. Phys. Lett.* **1998**, *72*, 915.
- (3) De Wolf, P.; Vandervorst, W.; Smith, H.; Khalil, N. *J. Vac. Sci. Technol. B* **2000**, *18*, 540.
- (4) Rawlett, A. M.; Hopson, T. J.; Nagahara, L. A.; Tsui, R. K.; Ramachandran, G. K.; Lindsay, S. M. *Appl. Phys. Lett.* **2002**, *81*, 3043.
- (5) Planès, J.; Houzé, F.; Chrétien, P.; Schneegans, O. *Appl. Phys. Lett.* **2001**, *79*, 2993.
- (6) Lin, H.-N.; Lin, H.-L.; Wang, S.-S.; Yu, L.-S.; Perng, G.-Y.; Chen, S.-A.; Chen, S.-H. *Appl. Phys. Lett.* **2002**, *81*, 2572.
- (7) Pingree, L. S. C.; Hersam, M. C.; Kern, M. M.; Scott, B. J.; Marks, T. J. *Appl. Phys. Lett.* **2004**, *85*, 344.
- (8) Pingree, L. S. C.; Martin, E. F.; Shull, K. R.; Hersam, M. C. *IEEE Trans. Nanotechnology* **2005**, *4*, 255.
- (9) Pingree, L. S. C.; Hersam, M. C. Submitted to *Appl. Phys. Lett.* (August 2005).
- (10) Bernanosé, A. *Brit. J. Appl. Phys. Suppl.* **1955**, *4*, S54.
- (11) Vityuk, N. V.; Mikho, V. V. *Sov. Phys. Semicond.* **1973**, *6*, 1479.

-
- (12) Vincent, P. S.; Barlow, W. A.; Hann, R. A.; Roberts, G. G. *Thin Solid Films* **1982**, *94*, 476.
- (13) Roberts, G. G.; McGinnity, M.; Vincent, P. S.; Barlow, W. A. *Solid State Commun.* **1979**, *32*, 683.
- (14) Tang, C. W.; Van Slyke, S. A. *Appl. Phys. Lett.* **1987**, *51*, 913.
- (15) Tang, C. W.; Van Slyke, S. A. *J. Appl. Phys.* **1989**, *65*, 3610.
- (16) In November 1997 Pioneer Co. Japan commercialized a monochrome 256 x 64 dot matrix OLED display for automotive applications.
- (17) Kubota, H.; Miyaguchi, S.; Ishizuka, S.; Wakimoto, T.; Funaki, J.; Fukuda, Y.; Watanabe, T.; Ochi, H.; Sakamoto, T.; Miyake, T.; Tsuchida, M.; Ohshita, I.; Tohma, T. *J. Lumin.* **2000**, *56*, 87–89.
- (18) Kido, J. *Phys. World* **1999**, *12*, 27.
- (19) Wakimoto, T.; Kawami, S.; Yonemoto, Y.; Murayama, R.; Funaki, J.; Sato, H.; Nakada, H.; Imai, K. International Symposium of Inorganic and Organic Electroluminescence, Hamamatsu, Japan, 1994.
- (20) Sato, Y.; Kanai, H. *Mol. Cryst. Liq. Cryst.* **1994**, *253*, 143.
- (21) Scott, J. C.; Kaufmann, J. H.; Brock, P. J.; Di Pietro, R.; Salem, J.; Goitia, J. A. *J. Appl. Phys.* **1996**, *79*, 2745.
- (22) Jonda, C.; Mayer, A. B. R. *Chem. Mater.* **1999**, *11*, 2429–435.
- (23) Li, W. J.; Wang, Q. W.; Cui, J.; Chou, H.; Shaheen, S. E.; Jabbour, G. E.; Anderson, J.; Lee, P.; Kippelen, B.; Peyghambarian, N.; Armstrong, N. R.; Marks, T. *J. Adv. Mater.* (Weinheim, Ger.) **1999**, *11*, 730.
- (24) Thompson, M. E.; Burrows, P. E.; Forrest, S. R. *Curr. Opin. Solid State Mater. Sci.* **1999**, *4*, 369.
- (25) Shao, R.; Kalinin, S. V.; Bonnell, D. A. *Appl. Phys. Lett.* **2003**, *82*, 1869.
- (26) O'Hayre, R.; Lee, M.; Prinz, F. B. *J. Appl. Phys.* **2004**, *95*, 8382.
- (27) Pingree, L. S. C.; Kern, M. M.; Scott, B. J.; Marks, T. J.; Hersam, M. C. *TMS Lett.* **2004**, *1*, 127.
- (28) Brütting, W.; Berleb, S.; Mückl, A. G. *Organic Electronics* **2001**, *2*.
- (29) Pingree, L. S. C.; Martin, E. F.; Shull, K. R.; Hersam, M. C. *IEEE Trans. Nano.* **2005**, *4*, 255.